Plasma Sources Sci. Technol. **7** (1998) 590–598. Printed in the UK PII: S0963-0252(98)97723-4

Surface temperature and thermal balance of probes immersed in high density plasma

R Piejak†, V Godyak†, B Alexandrovich† and N Tishchenko‡

† Osram Sylvania Inc., Beverly, MA 01915, USA
‡ Lawrence Livermore National Laboratory, Livermore, CA 94550, USA

Received 14 May 1998, in final form 24 August 1998

Abstract. The surface temperatures of thermal probes immersed in a low pressure inductively coupled argon discharge have been measured over a wide range of gas pressure. At a fixed discharge power, the measured temperature increases with gas pressure and decreases with increasing probe diameter. At a discharge power of 100 W, the surface temperature of a 0.4 mm diameter probe in the centre of the discharge ranges from 272 °C at 0.3 mTorr to 590 °C at 1 Torr. This temperature is considerably higher than the gas temperature. An analysis of the energy balance on a probe surface shows that plasma particle bombardment is the dominant heating process while radiation is the dominant cooling process. Probe temperatures found from an energy balance are in reasonable agreement with those measured in experiment.

1. Introduction

In practical applications of plasma discharge devices, there are times when it is important to know the surface temperature of an object immersed in the plasma. For example, in plasma processing it may be important to know the substrate temperature so that the substrate does not overheat during processing. This could also be an important issue in fluorescent lamps where a starting amalgam is immersed in plasma to dispense mercury into the lamp. Surface temperature is also an important consideration when immersing diagnostic probes or other materials into a low pressure plasma since the surface temperature may exceed the gas temperature and the immersed object may not be able to withstand these temperatures without degrading or contaminating the gas discharge.

A first approximation of the surface temperature is to assume the temperature of the object immersed in the discharge to be the gas temperature of the plasma. The gas temperature is generally determined from the balance between the energy transfer from electron collisions with gas atoms and the heat conduction from the discharge to the chamber surfaces. This approach provides a lower limit to the surface temperature and at gas pressures where thermal conduction is the dominant surface heating mechanism this estimate may be fairly accurate.

At low gas pressures and high plasma densities, however, thermal conduction may be a minor heat source to a surface and in this case the gas temperature may be considerably lower than the actual surface temperature. In this work the surface temperature of various diameter probes has been measured. It is the intent of this work to evaluate the various heating and cooling sources at a surface immersed in a low pressure argon discharge and to identify the dominant thermal processes.

2. Experimental set-up and temperature probes

Surface temperature and plasma parameter measurements were made in an inductively coupled RF discharge in argon at 6.78 MHz. An RF discharge was maintained by a five-turn pancake (flat) coil located below a stainless-steel cylindrical discharge chamber. The induction coil is air cooled with compressed air blown over the coil. As shown in figure 1, the coil was separated from the plasma by an electrostatic screen and a Pyrex disc that was 13 mm thick. Temperature probe and Langmuir probe measurements were made in the midplane of the discharge chamber. The discharge chamber has an inner diameter of 19.8 cm and a height of 10.5 cm. The chamber is pumped with a turbo-pump with a base pressure in the chamber in the 10^{-7} Torr range. During operation, argon flows through the system; a gas pressure controller (feedback system) keeps the gas pressure constant. Radial and axial directed ports on the chamber serve to support moveable temperature, Langmuir and magnetic probes.

Temperature measurements were made using commercially available fine gauge, unsheathed, chromel–alumel junction type thermocouples. The accuracy of the probes is about $\pm 1\%$ of reading $+1\,^{\circ}$C. Dimensions of the three

0963-0252/98/040590+09$19.50

Table 1. Dimensions of the three probes used in this work. Pyrex glass tubing was used in all cases.

Probe OD (mm)	Glass wall width (mm)	Thermocouple wire OD (μm)
0.4	0.05	25
1.2	0.1	25
6.3	1.0	250

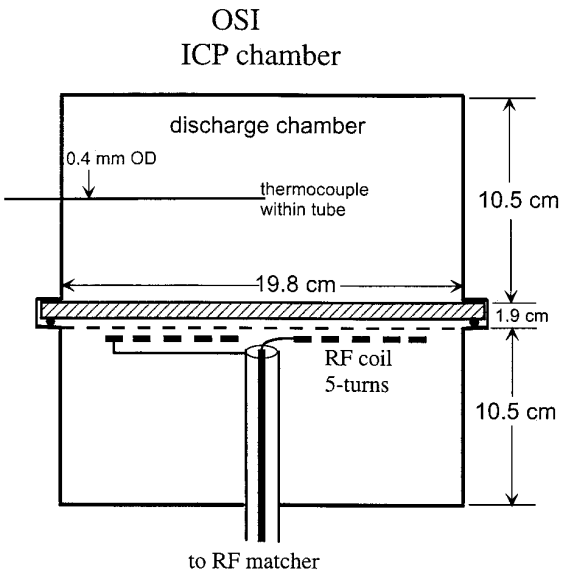

Figure 1. Schematic diagram of the experimental system.

probes used in this investigation are given in table 1. The majority of measurements were made with the 0.4 mm OD (smallest) probe. The general design guidelines for this probe were that it be small in size to minimize discharge perturbation and that it be constructed with thin walled glass tubing to minimize heat flow along the tube. Larger probes were also used to demonstrate the effect of probe perturbation. Essentially, all three probes consisted of a thermocouple within a Pyrex tube sealed at its end; thus the probe junction was electrically insulated from the plasma. Since the temperature measurements were made in an inductively driven RF discharge, a thermocouple display with high differential and common mode rejection was used so that the RF applied to the coil did not interfere with the temperature measurements. RF immunity of the thermocouple display and the Langmuir probe diagnostics was increased by practically eliminating the RF plasma potential with a planar electrostatic shield located between the driving coil and the plasma. The result of these precautions was that the probe temperature immediately after RF extinction was the same as that during the presence of RF.

Measurements were performed over a wide range of gas pressure between 0.3 mTorr and 1 Torr with RF power dissipation in the plasma of 100 W. To determine discharge power, the discharge electrical characteristics were measured and the power dissipated in the induction coil was subtracted from the total RF power delivered to the coil.

Table 2. Plasma and other related parameters on the centre axis in the discharge mid-plane at 100 W discharge power.

Parameter	1 mTorr	10 mTorr	100 mTorr
n (cm^{-3})	7.5×10^{10}	2.1×10^{11}	2.5×10^{12}
T_e (eV)	4.9	3.1	1.36
b/a	1.7	1.45	1.1
V_f (V)	20.4	13.4	6.2
T_g (°C)	213	111	262
T_s (°C)	275	338	532
$\tau(^1P_1)$ (s)	1.76×10^{-6}	3.1×10^{-5}	2.1×10^{-4}
$\tau(^3P_1)$ (s)	1.5×10^{-6}	2.9×10^{-5}	2×10^{-4}
λ_i (cm)	5.03	0.4	0.055
λ_g (cm)	8.6	0.84	0.086
T_s^{th} (°C)	221	254	454
$\langle P_e \rangle$ (W cm^{-3})	1.2×10^{-5}	1.57×10^{-4}	2×10^{-3}
$\langle P_i \rangle$ (W cm^{-3})	2.6×10^{-4}	1.36×10^{-3}	3.1×10^{-3}

3. Experimental results

3.1. Plasma parameters

Table 2 shows the plasma and other relevant parameters measured and calculated at the centre axis in the discharge midplane for a 100 W discharge. Both, the plasma density and effective electron temperature were obtained through integration of the EEDF measured with a Langmuir probe [1].

3.2. Probe temperature

Figure 2 shows the probe temperature measured in the mid-plane with the smallest probe (0.4 mm OD) two cm from the centre axis. Over the entire range of gas pressure, the temperature grows monotonically with pressure reaching 500–600 °C at gas pressures between 0.1 and 1 Torr. The probe temperature rises slowly with gas pressure at low and high pressures and rises relatively quickly at intermediate pressures (between 10 and 100 mTorr). The rapid temperature increase at intermediate pressures is mainly due to the dramatic rise in plasma density as gas pressure increases. The figure 'S' probe temperature dependence is attributed to the relatively weak plasma density dependence on gas pressure at low pressures and the rapid growth of radiation cooling at large probe temperatures.

Radial profiles of the probe temperature have been measured in the discharge midplane with the smallest probe and are shown in figure 3. At the lower gas pressures, the probe temperature profile has a wide peak about the discharge axis, while at 1 Torr the temperature profile peaks at 2 cm from the axis and falls more rapidly near the wall.

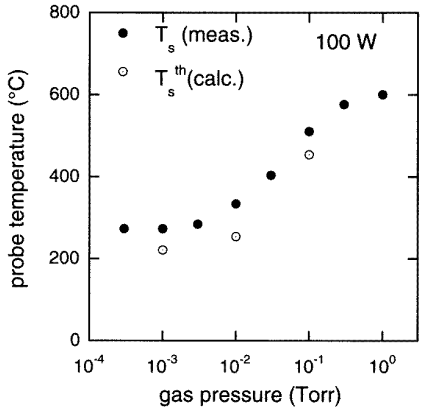

Figure 2. Probe temperature measured with 0.4 mm OD probe in mid-plane, 2 cm from centre axis for gas pressures between 0.3 mTorr and 1 Torr at 100 W discharge power is represented by black (solid) dots. The probe temperature, estimated from the analysis presented here, is given by open circles for 0.001, 0.01 and 0.1 Torr.

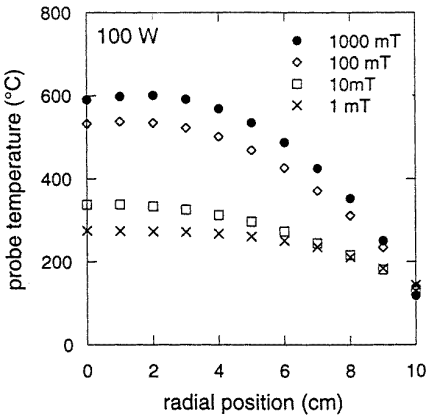

Figure 3. Radial profile of measured surface temperature with p = 1, 10, 100 and 1000 mTorr.

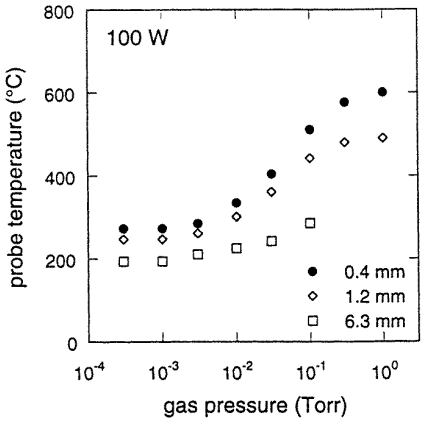

Figure 4. Measured surface temperature as a function of gas pressure for three different probe diameters.

The probe temperature appears to be correlated with the plasma density distribution. It is likely that this is a result of the non-uniform maintenance RF field created by the planar induction coil. At low gas pressure when the electron energy relaxation length λ_ε is larger than the characteristic plasma size, Λ (a condition of non-locality between the RF field and ionization), the plasma density distribution is practically independent of the spatial distribution of the RF field. This is similar to the free fall regime where the plasma density gradient is relatively small and thus the plasma density on its boundaries is rather appreciable [2]. In contrast, at high gas pressure when $\lambda_\varepsilon < \Lambda$ (nearing the condition of local coupling between RF field and ionization) the ionization profile tends to follow the RF field distribution and thus the plasma density maximum is shifted from the axis to the radius where the RF field is strongest. When gas pressure is high the plasma density on its boundaries is much smaller than its peak value.

3.3. Probe perturbation

It is well known from Langmuir probe studies that a body surrounded by plasma causes a local plasma perturbation. For a low pressure non-equilibrium gas discharge at gas pressures below a few Torr, the main effect of this disturbance is the depletion of the plasma around the probe [3]. This depletion reduces probe heating (and probe temperature) by the surrounding plasma. Plasma density depletion around the probe scales as a/λ_i, where a is the probe radius and λ_i is the ion mean free path. To neglect the plasma disturbance caused by the probe, its radius should be small compared to the ion mean free path ($a < \lambda_i$). For probes with $a = 0.2$ mm, this condition is satisfied below 200 mTorr in argon; therefore, probe temperature measured at pressures above 200 mTorr may be affected by the probe size.

To investigate the issue of local plasma perturbation we have measured probe surface temperature with larger diameter probes (1.2 and 6.3 mm OD). A comparison of the temperatures obtained with probes of differing diameters is shown in figure 4. As shown, a higher temperature is measured with smaller probes even at the lowest gas pressure when $a \ll \lambda_i$. The difference between temperatures measured with the smallest and the largest probes grows with gas pressure reaching a factor of two at gas pressure between 0.1 and 1 Torr. Besides the effect of plasma perturbation, the lower temperature obtained with larger probes may be attributed to thermal conduction along the probe holder. The ratio of glass cross section to probe surface of the 6.3 mm probe is 10 times larger than that of the 0.4 mm probe. As will be shown, the rise in probe temperature with reducing probe radius at $a \ll \lambda_i$ occurs because the probe sheath has an ion collection area that is larger than the probe itself.

The large probe perturbation effect caused by the presence of the 6.3 mm probe at a distance of 1 cm from the small 0.4 mm probe is shown in figure 5. Here the temperature difference of the small probe, with and without the large probe nearby, is given as a function of argon pressure. As expected, the temperature difference increases with gas pressure. Probe perturbation also increases with proximity of the large probe.

Experiments with different probes showed a very strong dependence between probe size and settling time. Settling

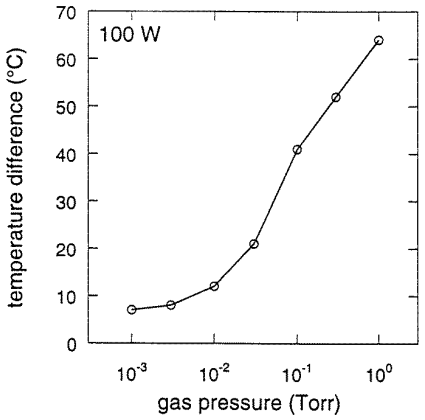

Figure 5. Perturbation due to the proximity of the large probe measured with the small probe.

time in this instance is taken to be the time it takes for the probe temperature to attain steady state after an abrupt change in discharge power. The settling time of the 0.4 mm probe was a few seconds while the settling times for the 1.2 mm and 6.3 mm probes were about 1 minute and 30 minutes, respectively. The difference in settling time is probably due to the difference in the probe's mass/surface ratio and the weak thermal coupling between the thermocouple wire and the glass shell of the large probes.

4. Energy balance on the probe surface

The temperature of a probe immersed in the plasma is determined by a variety of processes contributing to the energy balance at its surface. For a thin probe with negligible heat transfer along the probe holder, the steady state power balance equation at the probe surface is:

$$P_{pl} + P_{pr} + P_{ex} = P_r + P_c \tag{1}$$

where P_{pl}, P_{pr} and P_{ex} are the energy flux into the surface due to charged particles, plasma radiation and excited (metastable and resonant) neutral atoms, respectively, and P_r and P_c are the energy flux from the surface due to radiation and thermal conduction, respectively. In what follows the energy fluxes in equation (1) will be evaluated to determine the dominant terms in the probe power balance.

4.1. Charged particle bombardment

For plasma with a Maxwellian EEDF, the power flux density (W cm^{-2}) due to electron and ion bombardment to a cylindrical probe surface at the floating potential V_f is:

$$P_{pl} = 0.4n\frac{b}{a}\left(\frac{2T_e}{M}\right)^{1/2}[2T_e + \varepsilon_i + 0.5T_e + eV_f] \tag{2}$$

where

$$V_f = \frac{T_e}{2e}\left[\ln\frac{M}{2\pi m} - 2\ln\frac{b}{a}\right] \tag{3}$$

and n is the plasma density in the probe vicinity, ε_i is the ionization energy of argon (15.7 eV), T_e is the electron temperature in eV, M is the ion mass, m is the electron mass, e is the electron charge and b is the radius of the sheath surrounding the floating probe. In equation (2) the expression to the left of the brackets defines the ion and electron fluxes to the floating probe. The first term in the brackets is the average energy carried by the electrons that reach the probe's surface. The second term is the ionization energy released to the probe surface upon recombination, the third term is the initial ion energy at the plasma sheath interface and the fourth term is the ion energy gained in the sheath surrounding the floating probe.

The sheath radius b can be found by equating the ion current collected by the probe with that found from the Child–Langmuir law:

$$0.4ne\frac{b}{a}\left(\frac{2T_e}{M}\right)^{1/2} = \frac{4}{9}\varepsilon_0\left(\frac{2e}{m}\right)^{1/2}\frac{V_f^{1.5}}{a^2(-\beta^2)} \tag{4}$$

where ε_0 is the vacuum permittivity and $(-\beta^2)$ is a tabulated function of b/a in the Child–Langmuir law for concentric cylinders. From equation (4), the relation for b/a can be written as:

$$(-\beta^2)\frac{b}{a} = \frac{10}{9}\left(\frac{e}{T_e}\right)^{1/2}\frac{\varepsilon_0 V_f^{1.5}}{nea^2}. \tag{5}$$

For small probes and relatively low plasma density, which occurs at the lowest argon pressure, the ratio $b/a \gg 1$. Note also that for large probes and high gas pressures the plasma density around the probe may be significantly perturbed by the probe and could be smaller than its unperturbed value in the probe's absence.

4.2. Probe radiation cooling

Radiation cooling from the probe surface (W cm^{-2}) can be determined from Stefan's law:

$$P_r = \sigma(\xi_s T_s^4 - \xi_w T_w^4) \tag{6}$$

where σ is the Stefan–Boltzmann constant, $\sigma = 5.67 \times 10^{-12}$ W cm^{-2} K^{-4}, $\xi_s \approx 0.8$ for Pyrex [4] and $\xi_w \approx 1$ (ξ represents total hemispherical emissivity), T_s is the probe surface temperature and T_w is the chamber wall temperature. Although probe emissivity varies by a few per cent over the temperature range encountered here and the wall temperature is unlikely to be precisely constant, the small variations in these terms have been ignored. It is assumed that surface emissivity is unaffected by exposure to the plasma. In steady state, the temperature of the chamber wall T_w was measured to be about 60 °C at a discharge power of 100 W at 10 mTorr; this wall temperature was assumed at 1 and 100 mTorr.

4.3. Thermal conduction cooling

The surface of the probe is cooled by thermal conduction due to gas atoms striking the probe surface. In the generally encountered collisional regime, where the mean free path of the atom λ_g is much less than the probe diameter, heat

flux density is proportional to the local gradient of gas temperature and the gas thermal conductivity. In this case the heat flux to the probe can be written as:

$$P_{cond} = N_u k \frac{T_s - T_g}{2a} \tag{7}$$

where T_g is the gas temperature outside the boundary layer with thickness of about one probe diameter ($2a$), k is the thermal conductivity of the gas (1.6×10^{-4} W cm^{-1} K^{-1}) which is assumed to be independent of gas temperature and N_u is the Nusselt number (dimensionless thermal transfer coefficient). For this work the boundary layer is assumed to be free of convection around the probe and $N_u = 1$. Note that N_u may be much larger than one for a boundary layer with convection.

At gas pressures considered here (between 1 and 100 mTorr), however, the mean free path of a gas molecule, λ_g, is generally greater than, or equal to, the probe radius (0.2 mm). For this condition there is no boundary layer and an appropriate expression for heat flux is that for the free molecule regime rather than the collisional regime. In the free-molecule regime, heat flux is proportional to the temperature difference (not the gradient) between the probe surface temperature and the temperature of the surrounding gas and the thermal conductivity is proportional to the gas pressure. An expression for the heat flux density in the free-molecule regime is [5]

$$P_c = \alpha \chi p \left(\frac{273}{T_g}\right)^{1/2} (T_s - T_g) \tag{8}$$

where α is the accommodation coefficient, $\alpha = (T_r - T_g)/(T_s - T_g)$, χ is the free-molecule heat conductivity, T_r is the temperature of an atom after hitting the probe surface, T_g is the gas temperature in K just outside the probe surface and p is the gas pressure in Torr. The free molecule heat conductivity is [5]

$$\chi = 1.47 \times 10^2 M^{-1/2} (\gamma + 1)/(\gamma - 1) \text{ (W cm}^{-2} \text{ K}^{-1} \text{ Torr}^{-1}) \tag{9}$$

where γ is 1.67 for all noble gases and $\alpha = 0.86$ for argon [6]. Thus the free molecule heat conductivity for argon is $\chi = 9.26 \times 10^{-6}$ W cm^{-2} K^{-1} mTorr^{-1}.

4.4. Plasma radiation heating

Since the temperature probe is immersed in a gas discharge, there is a significant population of excited state atoms produced in the plasma and it is important to evaluate their contribution to probe heating due to plasma radiation. In the following two sections, the radiative energy transfer (this section) and the collisional energy transfer (next section) to the probe surface will be discussed. Energy transfer due to visible radiation from states above the resonant states is ignored because the photon energy is considerably less than VUV photons and the populations of these upper lying states are considerably less than the (lower lying) ^{1}P$_1$ and the ^{3}P$_1$ states.

In this section the radiation from the two resonance excited states of argon, ^{1}P$_1$ (also known as 4s[1/2]$_1$) and ^{3}P$_1$ (also known as 4s[3/2]$_1$), will be determined. The general procedure taken to evaluate probe surface heating due to resonance radiation is to determine the absorption coefficient for each resonant state and to determine the corresponding escape factor and the effective photon lifetime for each. From the measured electron energy distribution function, the rate coefficients for excitation and quenching of these states are determined. Finally, based on a particle balance equation for the (two) excited state densities, the population of the excited states is calculated and the radiation to the probe surface is determined.

To simplify the determination of the absorption coefficient for resonance radiation the dominant line broadening mechanism must be identified. There are three general causes of spectral line broadening: natural broadening (due to the natural radiated lifetime of the excited state), collisional broadening (due to collisions between excited states and electrons or heavy particles) and Doppler broadening (due to the velocity distribution of the emitting and absorbing atoms). Estimations of these effects show that Doppler broadening is the dominant broadening mechanism at the gas pressure and discharge conditions of this work. Therefore, only Doppler broadening will be considered in the following estimation of plasma radiation on the probe surface. In this case the absorption coefficient at line centre for a particular excited state is [7]

$$k_0 = \frac{\lambda^2}{4} \frac{g_*}{g_0} A N_g \frac{1}{\sqrt{\pi}\,\Delta\omega_D} \tag{10}$$

where $\Delta\omega_D$ is the Doppler width of the spectral line and is given by:

$$\Delta\omega_D = \frac{2\pi c}{\lambda} \sqrt{\frac{2k_B T_g}{Mc^2}} \tag{11}$$

and where λ is the transition wavelength, g_* is the statistical weight of the excited state ($g_* = 3$ for both resonance states), g_0 is the statistical weight of the ground state ($g_0 = 1$), A is the transition probability (Einstein coefficient), N_g is the number density of absorbing atoms, c is the speed of light and k_B is the Boltzmann constant. From spectroscopic data of transition probabilities [8], $A(^1\text{P}_1) = 5 \times 10^8$ s^{-1} and $A(^3\text{P}_1) = 1 \times 10^8$ s^{-1}.

Evaluating the absorption coefficients for 1, 10 and 100 mTorr it is found (using the temperature data in table 2) that for the ^{1}P$_1$ state k_0 increases from 17.2 cm^{-1} at 1 mTorr to 1490 cm^{-1} at 100 mTorr. Likewise, for the ^{3}P$_1$ state k_0 increases from 3.6 cm^{-1} to 314 cm^{-1}. Assuming the characteristic plasma dimension to be a few centimetres, $k_0 R$ is much greater than one and this suggests that the imprisonment time of the photons due to trapping is considerably larger than the natural lifetime and must be evaluated.

To determine the imprisonment time, the escape factor of a photon must be calculated. The escape factor is the probability that a photon covers path r without being absorbed [9]. Alternately, the escape factor may be thought of as the reciprocal of the number of emissions and absorptions of a photon prior to its escape from the discharge [10]. Normally for an arbitrary $k_0 R$ the escape

factor is expressed in integral form:

$$f(k_0 r) = \frac{2}{\pi}\int_0^\infty \exp(-x^2 - k_0 r \exp^{-x^2})\,\mathrm{d}x.$$

However, since $k_0 R \gg 1$, the escape factor can be evaluated from its asymptotic approximation [9]. Assuming an infinite cylinder with radius R (=10 cm) the escape factor may be expressed as:

$$\theta \approx \frac{\sqrt{\pi}}{4k_0 R\sqrt{\ln(k_0 R)}}. \tag{12}$$

The imprisonment time τ_i of a photon for a given excited state is then simply the product of the natural lifetime (A^{-1}) and θ^{-1}. Imprisonment times for the $^1P_1$ and the $^3P_1$ states are given in table 2.

Because of the large values of $k_0 R$ it is clear that the system considered here is optically thick and that considerable radiation trapping occurs. In this case the photon flux inside the bulk plasma is nearly uniform and the photon flux (per cm^2) can be estimated to be:

$$j \approx \frac{N_*}{k_0 \tau_i} \tag{13}$$

where N_* is the excited state density. To evaluate equation (13) the excited state density must be estimated. A two-level atom is assumed so that the excited state density can be easily estimated. In this case, the time rate of change of excited atoms $\partial N_*/\partial t$ is:

$$\frac{\partial N_*}{\partial t} = nN_g k_{gr} - nN_* k_{rg} - \frac{N_*}{\tau_i} \tag{14}$$

where k_{gr} is the rate coefficient (cm^{-3} s^{-1}) of excitation from the ground state and k_{rg} is the quenching rate coefficient found from the principle of detailed balance [11]. Equation (14) states that the time rate of change of the excited state density is equal to the rate of production of excited states directly from the ground state minus the rate of loss of excited states due to quenching collisions (collisions of the second kind) and radiative decay. In steady state the excited state density is:

$$N_* = \frac{n_e k_{gr} N_g}{\tau_i^{-1} + n_e k_{rg}}. \tag{15}$$

The rate coefficients k_{gr} and k_{rg} were determined for each excited state and each gas pressure by integrating the product of the measured electron energy distribution function, the electron velocity and the energy independent electron–neutral excitation cross section over the energy spectrum. Inserting the rate coefficients into equation (15) along with the corresponding imprisonment time and electron density, the excited state density for the $^1P_1$ and the $^3P_1$ were determined at 1, 10 and 100 mTorr. Knowing the excited state density for each resonant state, the corresponding photon flux can be determined from equation (13). The total photon energy flux absorbed by the probe surface is:

$$P_{pr} = \zeta_{ph} j_t \varepsilon \tag{16}$$

where ζ_{ph} is the probability that a photon is absorbed by the surface (taken to be one), j_t is the total radiation flux (sum of both resonant states) and ε is the average photon energy (11.8 eV). Expression (16) provides an upper limit appropriate for a probe immersed into the bulk plasma and positioned away from a plasma boundary. Values of P_{pr} based on equation (16) are presented in table 3 for different gas pressures. It is interesting that radiant power to the probe is highest at 10 mTorr.

4.5. Resonance and metastable atom heating

The final component of heating of the probe surface by excited states is due to the bombardment of the probe surface by resonance excited states $^1P_1$ and $^3P_1$ and the metastable states $^3P_0$ (also known as $4s[1/2]_0$) and $^3P_2$ (also known as $4s[3/2]_2$). Before this heat source can be considered it is necessary to estimate the metastable density.

As was done previously for the resonance population, the metastable population was also determined from a simple two level atom model. A steady-state particle balance equation which includes the production of metastables through electron-impact excitation (including cascades from the upper excited states) and the loss through ionization, quenching and diffusion loss to the walls can be written as:

$$N_m = \frac{N_e N_g k_{gm} \tau_d}{1 + N_e \tau_d (k_{ion} + k_{mg})} \tag{17}$$

where k_{gm} is an averaged rate coefficients for excitation to the metastable states, k_{ion} and k_{mg} are rate coefficients for ionization and quenching from the metastable state [12], respectively, and τ_d is the characteristic diffusion time for metastables leaving the system. Assuming a one-dimensional system and considering only the lowest order diffusion mode: $\tau_d = \Lambda^2/D$, where Λ is the characteristic length of the system and D is the metastable atom diffusion coefficient [9].

The power per unit area deposited on a surface due to bombardment by excited states (metastable and resonant states) can be written:

$$P_{ex} = 0.25\xi_m \varepsilon (N_m + N_*)\sqrt{\frac{8k_B T_g}{\pi M}} \tag{18}$$

where ξ_m is the probability of energy transfer to the surface and the metastable and resonant states are at the neutral gas temperature. Since the energies of the metastable and the resonant levels are so close in value, an average energy representing all four states was used to evaluate equation (18). The value of ξ_m strongly depends on surface material. However for this calculation it was assumed to be one (its maximum value). For catalytic active surfaces, like metals, $\xi_m = 0.1$–1, while for amorphous oxides, like glasses and ceramics, $\xi_m = 10^{-5}$–10^{-4} [13].

5. Gas temperature

To evaluate many of the preceding equations, it is necessary to know the gas number density N_g and temperature T_g

Table 3. The energy balance terms in equation (1) evaluated at 100 W discharge power. All terms are in W cm^{-2}. In calculation of P_{ex} and P_{pr}, it was assumed that $\xi_m = \zeta_{ph} = 1$. The calculation of P_c is based on free molecule conductivity.

Energy balance term	1 mTorr	10 mTorr	100 mTorr
P_{pl}	0.2	0.28	1.2
P_r	0.35	0.57	1.8
P_c	3.9×10^{-4}	0.015	0.15
P_{pr}	0.02	0.095	0.044
P_{ex}	5×10^{-4}	3.5×10^{-5}	2.4×10^{-3}

surrounding the probe. N_g is obtained directly from T_g. T_g can be estimated by considering the gas heating and cooling processes in the discharge chamber. In a low pressure gas discharge, gas heating is mainly provided by electron–atom elastic collisions and by ion–atom charge exchange collisions.

The power spent by an electron colliding with a gas atom is the product of the energy of the electron, the fraction of energy lost by the electron per collision and the number of collision per electron per second. The energy of a particular electron with velocity v is $1/2mv^2$, the fraction of energy lost per collision is $(2m/M)[1 - E_1/E_2]$ where E_1 is the mean energy per atom ($\frac{3}{2}k_BT_g$) and E_2 is the electron's kinetic energy, and the number of collisions per electron per second is $N\sigma(v)v$ where $\sigma(v)$ is the electron–neutral cross section for momentum transfer. Since the electrons possess a distribution of velocities, the average power dissipated per electron per second is obtained by integrating (over velocity space) the product described above together with the electron velocity distribution function (evdf). The evdf is assumed to be isotropic and Maxwellian with an electron temperature (measured with a Langmuir probe) given in table 2. For elastic collisions, the (assumed) Maxwellian distribution gives the same result as the measured EEPF. An assumed Maxwellian distribution (rather than the measured one) was used here because it made it easier to evaluate equation (19). Thus the integral for the average power dissipated deposited into the gas by electrons is:

$$P_e = N_g\left(\frac{m^2}{M}\right)\int_0^\infty \sigma(v)\left[1 - \frac{3k_BT_g}{mv^2}\right]v^3 f(v)\,\mathrm{d}v \qquad (19)$$

where

$$f(v) = 4\pi v^2\left(\frac{m}{2\pi T_e}\right)^{3/2}\exp\left(\frac{-mv^2}{2T_e}\right).$$

The ion–atom power heating per unit volume is:

$$P_i = F_i v_i P_{ic} = enE\left(\frac{2e\lambda_i E}{\pi M}\right)^{1/2}\left[1 - \exp\frac{-(d-x)}{\lambda_i}\right] \qquad (20)$$

where $F_i = enE$ is the electric force acting on ions per unit volume, $v_i = (2e\lambda_i E/\pi M)^{1/2}$ is the ion velocity in the ambipolar field E and $P_{ic} = 1 - \exp(-(d-x)/\lambda_i)$ is the probability that an ion transfers its charge to a gas atom prior to reaching the wall. Note that in argon at $pd < 1$ Torr cm, the ion ambipolar velocity v_i exceeds the ion thermal velocity v_{iT} over most of the discharge volume (the variable ion mobility regime in a strong electric field). Starting with v_{iT} at the discharge centre, the ion velocity can reach the ion sound speed $v_s = (T_e/M)^{1/2} \gg v_{iT}$ at the plasma boundary ($x = d$). The ambipolar field is defined by the electron temperature and by the plasma density profile, $E = (T_e/ne)\,\mathrm{d}n/\mathrm{d}x$, thus, for a 1D plasma profile:

$$P_i = \left(\frac{2\lambda_i}{\pi Mn}\right)^{1/2}\left(T_e\frac{\mathrm{d}n}{\mathrm{d}x}\right)^{3/2}\left[1 - \exp\frac{-(d-x)}{\lambda_i}\right]. \qquad (21)$$

An estimate of P_i/P_e gives:

$$P_i/P_e \approx (M/m)^{1/2}\lambda_e\lambda_i^{1/2}\Lambda^{-2/3} \propto (p\Lambda)^{-2/3} \qquad (22)$$

for $\lambda_i < \Lambda$, where Λ is the plasma characteristic size. Evaluation of equation (22) shows that electron heating prevails at high gas pressure while ion heating is dominant at low gas pressure. Note that equation (20) implies collisional ion motion ($\lambda_i < \Lambda$) and has its maximum at $p \approx 1$ mTorr where $\lambda_i \approx \Lambda$. At lower gas pressure, P_i should diminish due to a transition of ion motion to the free fall (collisionless) regime. This is accounted for by the probability factor in equation (21).

In steady state, gas heating must be equal to the heat transferred to the chamber wall. Depending on the gas pressure this transfer can be collisionally dominated (diffusional regime at $\lambda_g < \Lambda$) or collisionless (free molecule regime at $\lambda_g > \Lambda$); for argon $\lambda_g = \Lambda$ at $p \approx 3$ mTorr.

The gas temperature at the axis of the discharge chamber can be estimated in the diffusional regime by solving the heat transfer equation:

$$\nabla^2 T_g + \frac{P_g}{k} = 0 \qquad (23)$$

where $P_g = (P_e + P_i)$ and k is the thermal conductivity of argon. To solve equation (23), k is assumed constant and the two-dimensional geometry of the discharge chamber is reduced to one dimension by equating the characteristic length Λ of the fundamental diffusional mode for the two-dimensional problem to a corresponding length of the one-dimensional problem with reduced wall separation $L_0 = 2d$. Thus, $(\pi/L)^2 + (2.405/R)^2 = \Lambda^{-2} = (\pi/L_0)^2$; $L_0 = 8.1$ cm and $\Lambda = 2.58$ cm; i.e., the discharge chamber is considered to act as a gap between two infinite parallel plates separated by 8.1 cm. P_e and P_i averaged over the discharge are given in table 2. At gas pressures of 100 and 10 mTorr $\lambda_g < \Lambda$ and equation (23) is used to determine gas temperature shown in table 2.

At 1 mTorr, $\lambda_g > \Lambda$ and a free molecule thermal conductivity was used to determine the gas temperature. In this case, heat (energy) is transferred from the gas to the wall. The gas temperature is assumed to be uniform and is found by equating the total energy per cm^2 dissipated in the gas (due to ion heating) with the heat flux to the wall. The energy transferred per cm^2 is simply the number of atoms hitting the surface ($0.25N_g v_{gas}$) times the energy transfer per collision ($2k_B[T_g - T_w]$). This value for the energy transfer per collision assumes that a gas atom rebounds from a wall at the wall temperature and thus results in a lower limit of gas temperature due to ion heating. An equation describing the heat transfer similar in form to equation (8) can be written:

$$\chi p\left(\frac{273}{T_g}\right)^{1/2}(T_g - T_w) = \int_0^d P_i \,\mathrm{d}x \tag{24}$$

where T_w is the wall temperature. To determine P_i the plasma density distribution was assumed to be parabolic with a non-zero boundary value:

$$n = n_0\left[1 - (1-h)\frac{x^2}{d^2}\right] \tag{25}$$

where h is the relative plasma density on its boundary corresponding to the variable mobility model [14, 15] applicable when $\lambda_i/d \leq T_g/T_e$.

$$h = 0.86\left[3 + \frac{d}{\lambda_i}\right]^{-1/2}. \tag{26}$$

6. Probe temperature calculation

The calculation of the terms in the energy balance equation (1) are given in table 3 and show that in this experiment the bulk of the probe heating is due to plasma bombardment given by equation (2) while the main cooling is due to radiation given by equation (6). Therefore, the probe surface temperature can be roughly estimated by reducing the equation of the energy balance on the probe surface to include only these (two) terms such that:

$$\sigma(\xi_s T_s^4 - \xi_w T_w^4) = 0.4n(b/a)(2T_e/M)^{1/2}[2.5T_e + \varepsilon_i + eV_f]. \tag{27}$$

The values of probe temperature T_s^{th} found from equation (27) for a 100 W argon discharge are given in table 2 and shown in figure 2. They demonstrate a plausible agreement with the measured temperatures T_s and, in conjunction with the calculated gas temperature, suggest that one should indeed expect that the surface temperature should be somewhat independent of the gas temperature. On the other hand, as one can see in table 3 the calculated plasma heating power P_{pl} is 30–50% less than the probe radiation power P_r calculated using the (measured) value T_s. This discrepancy could be explained by plasma depletion caused by the probe as well as by the many assumptions made in evaluating the energy transfer processes. Fortunately, the fourth power of the temperature in the Stefan law governing radiational cooling makes the probe temperature rather insensitive to the heat input. For $p = 10$ mTorr, the contribution of P_{pr} (0.095 W cm^{-2}) would change the calculated T_s^{th} by 13%. Therefore, equation (27) reasonably estimates the surface temperature of a small cylindrical tube immersed in a high density, low pressure gas discharge.

7. Conclusions

The temperature of various size temperature probes immersed in the dense plasma of an inductively coupled argon discharge has been measured over a wide range of gas pressure. Unexpected high probe temperatures (500–600 °C) at very modest discharge power were found for argon pressures between 0.1 and 1 Torr. This brings forth concerns for the material integrity in the design of Langmuir and magnetic probes. It has been found that at a fixed discharge power the probe temperature grows with gas pressure and falls with the probe diameter, the latter being due to a plasma density perturbation caused by the presence of the large probe body.

The analysis of the energy balance for neutral gas showed that at low gas pressures, typical for plasma processing devices, the main gas heating mechanism is due to ion charge-exchange collisions resulting from a relatively large ambipolar ion drift velocity. The energy balance for the probe surface has been analysed and different processes affecting the probe temperature have been evaluated. It has been found that in a low pressure inductive RF discharge (or other plasma source with similar gas pressure, volume and discharge power) the dominant surface heating process is plasma particle bombardment and the dominant surface cooling process is radiational cooling. Therefore, the balance between these processes largely determines surface temperature. Since plasma heating is proportional to electron density and the electron density is proportional to discharge power, one could expect the surface temperature to be proportional to discharge power raised to the 1/4 power.

An analytical expression (equation (27)) has been obtained which relates the temperature of a probe immersed into the plasma to some of the plasma parameters. The probe temperatures found from equation (27) are in reasonable agreement with those measured in experiment. This formula can be helpful in estimating the working temperature of Langmuir and magnetic probes for diagnostics of high density plasma.

References

[1] Godyak V 1996 *ESCAMPIG 96 (Bratislava, 1996)* vol 20E, part A (European Physics Society) ed Lukac, Kosinar and Skalny, pp IX–XII

[2] Kolobov V I and Godyak V A 1995 *IEEE Trans. Plasma Sci.* **23** 503

[3] Waymouth J F 1964 *Phys. Fluids* **7** 1843

[4] Touloukian Y S and DeWitt D P 1972 *Thermophysical Properties of Matter* vol 8 (IFI–Plenum) p 1579

[5] Dushman S 1962 *Scientific Foundations of Vacuum Techniques* 2nd edn, ed J M Lafferty (New York: Wiley)

[6] Leek J H 1957 *Pressure Measurements in Vacuum Systems* (London: Institute of Physics)

[7] Holstein T 1947 *Phys. Rev.* **72** 1212

Biberman L M 1947 *Sov. Phys.—JETP* **17** 416
Biberman L M 1949 *Sov. Phys.—JETP* **19** 584
[8] Radtsig A A and Smirnov B M 1985 *Reference Data on Atoms, Molecules, and Ions* (Berlin: Springer)
[9] Smirnov B M 1977 *Introduction to Plasma Physics* (Moscow: MIR)
[10] Holstein T 1951 *Phys. Rev.* **83** 1159
[11] Raizer Y P 1991 *Gas Discharge Physics* (New York: Springer)
[12] de Heer F J 1979 *J. Phys. B: At. Mol. Phys.* **12** 979
[13] Magunov A 1996 private communications
[14] Godyak V A and Maximov V N 1977 *Vestnik Moskovskogo Universiteta, Ser. Fiz. Astr.* **18** 51 (in Russian)
[15] Lieberman M A and Lichtenberg A J 1994 *Principles of Plasma Discharge and Materials Processing* (New York: Wiley–Interscience)